Macromolecules

pubs.acs.org/Macromolecules Article

Monomer Sequence Effects on Interfacial Width and Mixing in Self-Assembled Diblock Copolymers

Anastasia L. Patterson, Beihang Yu, Scott P. O. Danielsen, Emily C. Davidson, Glenn H. Fredrickson, and Rachel A. Segalman*

Cite This: *Macromolecules* 2020, 53, 3262−3272 Read Online

ACCESS | Metrics & More | Article Recommendations | Supporting Information

ABSTRACT: Monomer sequence is shown to directly control interfacial and in-domain mixing in lamellar polystyrene-*b*-polypeptoid diblock copolymers, where the polypeptoid block is composed of precise sequences of highly segregating (polar) and compatibilizing (nonpolar) repeat units. With monomer-by-monomer sequence control, the effects of blockiness, comonomer distribution, and taper direction on the interfacial width are measured with small-angle X-ray scattering and further understood through simulations with self-consistent field theory. When compatibilizing groups are distributed along the polypeptoid chain, the presence of neighboring polar groups suppresses interfacial mixing and causes the interfacial width to narrow, especially for the blocky sequence. When compatibilizing groups are tapered from the block junction, they are strongly localized at the domain interface and both interfacial mixing and interfacial width are increased. Consequently, tapered sequences produce more pure domain centers, while the distributed materials have compatibilizing groups located throughout the polypeptoid domain, encouraging more polystyrene to mix in. An analogous poly(*n*-butyl acrylate) system was synthesized to probe the effects of a different interaction parameter (χ). Similar trends with sequence were found but with smaller magnitudes due to the higher χ. This study shows that monomer sequence directly affects segmental mixing both at and away from the interface, with consequences for interfacial width and domain spacing. Along with the sequence-driven nonideal chain conformations shown recently, these combined sequence-specific effects determine the resulting geometry and thermal stability of the self-assembled lamellae, suggesting that comonomer sequence can be used to tailor self-assembling materials without changing the composition or chemistry.

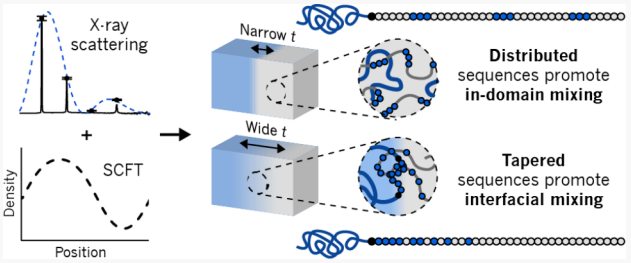

INTRODUCTION

Understanding the interface between dissimilar components of block copolymers is key to designing materials for self-assembly, blend compatibilization, and surfactants, where tethering across a high-surface-tension interface is desirable for high-performance materials.[1−7] In bulk self-assembled block copolymers, the composite-like mechanical properties rely on the segregation of distinct domains and are strongly influenced by the character of the interface between them, whether sharp or mixed.[8−10] Furthermore, self-assembling block copolymers are useful for applications that require patterning on nanometer length scales, where the fidelity of the pattern is partly determined by the sharpness of the interface between distinct domains.[11−13]

In all of these applications, the chemistry of the components can be modified to tune the segregation strength across the interface, which strongly influences the interfacial tension and width as well as the phase stability. Tuning the segregation strength is often done through choosing systems with large block−block interaction parameters (high χs),[14−16] introducing specific interactions,[17] or blending in judicious additives.[18−21] Controlling comonomer sequence is a promising tool to tune the mixing thermodynamics of dissimilar components without changing the chemistry or composition,[22] but synthetic routes that facilely allow for sequence control are relatively new. Semibatch methods to produce tapered and gradient composition profiles have been shown to affect the properties of self-assembled melts (influencing thermal phase stability, phase windows, glass transition temperatures, and interfacial widths) as well as enhance blend compatibilization.[23−30] X-ray reflectivity studies of forward and inverse tapers in polystyrene−polyisoprene (PS−PI) diblock copolymers found that, for the same overall composition and molecular weight, the inverse taper has a larger interfacial thickness than the forward taper (10.5 nm versus 5.2 nm, respectively).[26] In addition to these effects arising from varying composition profiles over segments of the polymer chain,

Received: November 19, 2019
Revised: April 13, 2020
Published: April 27, 2020

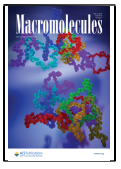

https://dx.doi.org/10.1021/acs.macromol.9b02426
Macromolecules 2020, 53, 3262−3272

simulations predict that sequence control on even the monomeric scale determines the self-assembled phase behavior.[31−33] However, the semibatch synthetic strategy cannot produce monomer-length-scale sequence definition, so the effects of finely controlled comonomer sequence are relatively unexplored.

With monomer-level sequence control and versatile chemistry, polypeptoids (N-substituted polyglycines) are emerging materials for studying the role of precise monomer sequence in polymer systems with no compositional dispersity. With the precise control enabled by polypeptoids, monomer sequence has been shown to affect the melting and crystallization of polymers[34] as well as block copolymer microphase separation that impacts material properties like conductivity.[35−42] Recent work utilized sequence-defined polypeptoids in lamellae-forming polystyrene-*b*-polypeptoid diblock copolymers to study the influence of compatibilizing comonomer sequence on self-assembly.[43] Styrene-like repeat units were incorporated into the polypeptoid block in precise sequences with polar repeat units, compatibilizing the polypeptoid to polystyrene. It was found that the sequence of compatibilizing comonomers significantly impacts domain spacing, hypothesized to be due to nonideal chain conformations driven by localization of compatibilizing groups at the block−block interface as supported by simulations with self-consistent field theory. Further, the interaction parameter between blocks was clearly affected, evidenced by order−disorder transitions varying up to 10 °C with sequence variation alone. Interestingly, the interaction parameter (χ) is known to vary inversely with a geometric property of the self-assembled system: interfacial thickness (t). This relationship scales as $t \approx \chi^{-\alpha}$, where in the limit of infinite molecular weight homopolymers, the scaling exponent α is 1/2, and for block copolymers with finite molecular weights subject to fluctuation effects, $\alpha \approx \frac{5}{6}$ in the range of physically relevant χ values ($\chi \ll 1$).[44−47] Recent work utilizes this relationship to directly estimate the segregation strength χN by comparing measured and simulated interfacial widths.[48] Higher χ leads to larger enthalpic mixing penalties and narrower interfaces, and given the range of order−disorder transition temperatures observed in the sequence-defined polystyrene-*b*-polypeptoid system, it is expected that these materials will display a corresponding range of interfacial thicknesses. While it was found that sequence-specific analyses must be employed to quantify χ differences arising from monomer sequence,[43] the differences in segregation strength implied by the different order−disorder transition temperatures are likely to manifest as a variation in interfacial thickness at fixed chain length and composition. This paper details further analysis on these same sequence-defined polystyrene-*block*-polypeptoid diblock copolymers, and this analysis is extended to a new, analogous poly(*n*-butyl)acrylate series to explore the effects of the interaction parameter χ.

Here, it is shown that controlling the sequence on the monomer length scale affects the interfacial thickness of lamellar polystyrene-*b*-polypeptoid diblock copolymers, where the polypeptoid block is either a homopolymer of polar ether side chains or a sequence-defined copolymer of the polar side chains with compatibilizing phenyl side chains (Figure 1). The tapered sequences have wider interfacial widths due to a higher content of compatibilizing groups at the interfaces. The distributed sequences have more compatibilizing groups in the domain centers, leading to less interfacial mixing but more in-domain mixing of polystyrene and thus swollen polypeptoid domains. In short, mixing is more favored where there are compatibilizing groups, and localization of these groups is set by the primary monomer sequence. In an analogous poly(*n*-butyl acrylate)-*b*-polypeptoid system, there are similar trends with sequence but with smaller absolute variation due to a higher interaction parameter χ, highlighting the utility of lower χ systems when exploiting sequence effects. The result on tapered sequences in this work contrasts to prior work on tapered block copolymer systems,[26] highlighting the effects of precise monomer sequence without compositional dispersity on the interfacial width.

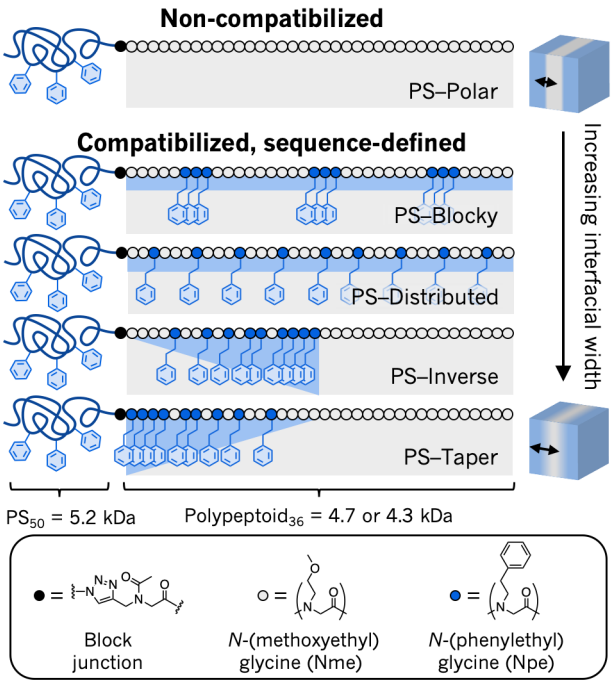

Figure 1. Summary of polystyrene-*b*-polypeptoid materials. Non-compatibilized diblock copolymer (top, PS−Polar) and four sequence-defined diblock copolymers with identical composition and degree of polymerization (bottom four) were synthesized.

METHODS

Synthesis and Characterization of Polystyrene− and Poly(*n*-butyl acrylate)−Polypeptoid Diblock Copolymers. Synthesis and characterization procedures were detailed in a recent paper.[43] In short, styrene and *n*-butyl acrylate were polymerized via atom-transfer radical polymerization, and the bromide chain end was substituted with sodium azide. The resulting azide-functionalized polymers were characterized with gel permeation chromatography (GPC), where polystyrene (PS) was measured against polystyrene standards and poly(*n*-butyl acrylate) (PnBA) was measured against poly(methyl methacrylate) standards and converted with Mark−Houwink parameters for low molecular weight poly(*n*-butyl acrylate).[49] Polypeptoids were synthesized via the solid-phase submonomer method[50] with polar side chains (from *N*-methoxyethylamine, "Nme") and nonpolar side chains (from *N*-phenylethylamine, "Npe"), with an additional terminal unit incorporating an alkyne side chain. Polypeptoids were analyzed with matrix-assisted laser desorption ionization mass spectrometry (MALDI-MS) and ultra-performance liquid chromatography mass spectrometry (UPLC-MS) (ref 43). Azide-terminated polystyrene (PS−N_3) or poly(*n*-butyl acrylate) (PnBA−N_3) was conjugated to alkyne-terminated polypeptoid using copper-mediated azide−alkyne click chemistry, and

https://dx.doi.org/10.1021/acs.macromol.9b02426
Macromolecules 2020, 53, 3262−3272

excess homopolymer was removed via precipitation and preparatory GPC (PS) or column chromatography on alumina (PnBA). See ref 43 for chromatography analysis of polypeptoids, Figures SI-1−3 for GPC and MALDI spectra, and Table 1 for a summary of characteristics of the synthesized blocks.

Table 1. Characteristics of Constituent Blocks

block identity	block name	M_n (g mol^{-1})	$Đ$	density (±0.02, g cm^{-3})
polystyrene	PS−N_3	5200	1.12[a]	1.03
poly(*n*-butyl acrylate)	PnBA−N_3	4900	1.15[a]	1.03
compatibilized copolypeptoid	$Nme_{27}Npe_9$−≡	4712	<1.04[b]	1.26
homopolypeptoid	Nme_{36}−≡	4296	<1.04[b]	1.26

[a]Dispersities ($Đ$) were measured with GPC. [b]Dispersities ($Đ$) were measured with UPLC-MS.

Pycnometry. Polystyrene, poly(*n*-butyl acrylate), and polypeptoid samples were thermally annealed above their glass transition temperatures in high vacuum (3×10^{-8} Torr) before cooling slowly to room temperature, producing glassy solids devoid of air bubbles. Sample volumes were measured at room temperature with a Micromeritics AccuPyc II 1340 gas pycnometer using the gas displacement technique with helium. Five purge cycles were followed by five measurements. Sample densities are calculated from the obtained average volume and separately measured masses.

Small-Angle X-ray Scattering (SAXS). Diblock copolymers were loaded into aluminum washers sealed on one side with Kapton tape, with nonadhesive Kapton film blocking the adhesive in the center. Samples were thermally annealed at 170 °C for at least 3 h under vacuum at 3×10^{-8} Torr, cooled slowly (≤1 °C min^{-1}) to 110 °C, and annealed overnight before cooling slowly to room temperature in vacuum, removing, and sealing the other side of the washer. Small-angle X-ray scattering (SAXS) was performed at the National Synchrotron Light Source II (NSLS-II, Brookhaven National Lab) at beamline 11-BM, configured with an X-ray energy of 13.5 keV and sample−detector distance of 3 m, and at the Advanced Light Source (ALS, Lawrence Berkeley National Lab) at beamline 7.3.3, configured with an X-ray energy of 10 keV and sample−detector distance of 3.5 m. All measurements of self-assembled materials are from NSLS-II and are reported at room temperature. Data were calibrated with silver behenate standards, reduced using circular averaging, and corrected for empty cell scattering and q-independent background scattering (approximated as a constant fit to high q). The measured intensity reflects the structure of many lamellar grains (the beam size is 200 μm × 200 μm, and sample thickness is 800 μm), producing 1D scattering with good statistics and at least two higher order reflections for all samples ($2q^*$ and $3q^*$). Data from the ALS were reduced as above using the Nika package for Igor Pro.[51]

Self-Consistent Field Theory (SCFT). Simulations were performed using a previously reported SCFT framework for sequence-defined block copolymers.[36] Polystyrene−polypeptoid materials were modeled as incompressible melts of discrete Gaussian chains;[52] the sequence-defined polypeptoid block was represented with one bead per residue, while the PS block was represented with one bead per reference volume of 0.1 nm^3 and elaborated to a block of 50 beads to match the measured molecular weight and density. The interaction parameters between polar polypeptoid, nonpolar polypeptoid, and PS are defined with three binary χ values, where χ_{PS-Nme}:χ_{PS-Npe}:$\chi_{Nme-Npe}$ is 1.0:0.8:0.2. χ_{PS-Nme} and χ_{PS-Npe} were measured at 220 °C via application of the random phase approximation to SAXS curves of the disordered melt for PS−Polar and PS−Nonpolar.[43] The polar−nonpolar polypeptoid interaction parameter $\chi_{Nme-Npe}$ was estimated based on ref 40 and by comparing SCFT predictions to experiment. Density profiles reported here are shown at $\chi_{PS-Nme}N$ = 20 unless otherwise noted, which is the segregation strength that best matches the experimentally determined ratio of interfacial thickness to domain spacing ($t/d \approx 0.25$).

Simulations were performed with periodic boundary conditions and cell relaxation via a variable cell technique.[53] The integrodifference equations associated with forward and backward chain propagators were solved pseudospectrally.[54,55] Fields were relaxed to saddle-point configurations using a semi-implicit scheme.[52,56]

Lamellar Model with Diffuse Interfaces. The scattering from a two-component lamellar material with diffuse interfaces is derived below, following Roe, Beckingham et al., and Burns et al.[48,57,58] This approach for measurement of the interfacial widths utilizes peak intensities from well-defined scattering peaks rather than the historically used high-q scattering tail,[59,60] as it is less prone to error from subtracting the unknown background.

Consider a perfectly oriented, one-dimensional lamellar stack with alternating domains of components A and B. This structure contributes to the scattering intensity as

$$I_{\text{ideal, 1D}}(q) \approx (\Delta\rho)^2 \sin^2\left(\frac{qd_A}{2}\right)q^{-2} \tag{1}$$

where $\Delta\rho$ is the difference in scattering length density (related to electron density contrast) between the two domains and d_A is the thickness of layer A (it will be shown that either d_A or d_B can be chosen without loss of generality).

In real systems, there are many grains of lamellar structures randomly oriented in three dimensions, and the scattering measured is the 1D scattering multiplied by the Lorentz correction q^{-2},[61,62] yielding the familiar Porod decay of q^{-4}

$$I_{\text{ideal,isotropic}}(q) \approx (\Delta\rho)^2 \sin^2\left(\frac{qd_A}{2}\right)q^{-4} \tag{2}$$

Equation 2 represents the azimuthally averaged isotropic scattering of randomly oriented lamellar sheets and is "ideal" in that it has perfectly sharp interfaces (modeled as step functions in scattering length density, Figure 2a). A correction must be made to account for diffuse

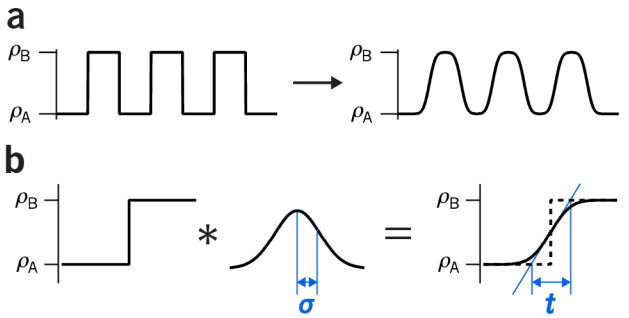

Figure 2. (a) Ideal density profile has smooth transitions between components due to interfacial mixing. (b) Interfacial mixing is modeled by the convolution of the ideal (step-function) change in scattering length density (top) with a Gaussian smoothing function with variance σ^2, yielding a smooth variation in electron density in the interfacially mixed region (mathematically an error function, bottom), with interfacial thickness $t = \sqrt{2\pi}\sigma$.

interfaces at the lamellar domain boundaries, where there is some degree of mixing between dissimilar blocks. This interfacial mixing is modeled by convoluting a smoothing function (often chosen to be Gaussian) with the ideal, sharp interface to create a smoothly varying scattering length density profile. The Fourier transform of this real-space Gaussian smoothing leads to a Gaussian-like decay in q space of the structure factor, modifying the ideal q^{-4} behavior as

$$I_{\text{diffuse,isotropic}}(q) \approx (\Delta\rho)^2 \sin^2\left(\frac{qd_A}{2}\right)q^{-4}e^{-\sigma^2q^2} \tag{3}$$

https://dx.doi.org/10.1021/acs.macromol.9b02426
Macromolecules 2020, 53, 3262−3272

where σ^2 is the variance of the real-space Gaussian. Equation 3 describes the envelope in which scattering peak intensities will be found for a real lamellar material with diffuse interfaces.

Peaks only occur when the Bragg condition $q = \frac{2\pi n}{d}$ is met, where $d = d_A + d_B$ is the full lamellar domain spacing. The intensity of peaks of order n then go as

$$I_{\text{diffuse,isotropic}}(n) \approx (\Delta\rho)^2 \sin^2(\pi n \phi_A) n^{-4} e^{-2\pi n^2 (t/d)^2} \quad (4)$$

where $\phi_A = d_A/d$ is the volume fraction of domain A and t is the interfacial thickness, related to σ as $t = \sqrt{2\pi}\sigma$. Interfacial thickness t as defined here is illustrated in Figure 2b and calculated as the width between the intersections of the pure component densities with the line tangent to the density profile at the interface

$$t = \Delta\rho \left(\left. \frac{d\rho}{dx} \right|_{x_{\text{interface}}} \right)^{-1} \quad (5)$$

Since $\sin^2(z)$ is even around $z = \pi/2$, the argument $\pi n \phi_A$ is equivalent whether A is chosen such that $\phi_A > 1/2$ or $\phi_A < 1/2$; this is Babinet's reciprocity theorem. For consistency, we set $\phi_A = \phi_{\text{peptoid}} < 1/2$ throughout this paper (where ϕ_{peptoid} is the volume fraction of the polypeptoid-rich domain). Equation 4 can be used directly to describe peak intensities from isotropic lamellar scattering, where d is calculated from the primary scattering peak position as $d = 2\pi/q^*$. Note that the exponential term in eq 4 is equivalent to a Debye–Waller factor, which describes Gaussian fluctuations in the position of a sharp interface. The measured interfacial thickness t then may arise from both segmental mixing and fluctuations. In this study, the interfacial thickness is measured at a temperature far from the order–disorder transition, so it is assumed that most of the measured interfacial thickness arises from segmental mixing.

Fitting to the Diffuse Interface Model. The area of each scattering peak was found by fitting individual Voigt peaks[63] with a local linear baseline that accounts for unknown background; sensitivity analyses show that the choice of baseline leads to a <5% variation in peak area, which creates only a 1% variation in interfacial width. In applying a diffuse interface model for two-component lamellar materials (eq 4), interfacial thickness (t) and relative domain size (ϕ_{peptoid}) were allowed to vary as well as a constant scaling factor that accounts for the use of arbitrary units of intensity.

By comparing the sharp interface model (eq 3) and diffuse interface model (eq 4) against measured peak intensities, it is clear that the materials studied here are much better modeled with a diffuse interface, as demonstrated with Porod-corrected scattering ($I(q)*q^4$) of an example material (PnBA–Polar, Figure 3). Variation in the volume fraction of the polypeptoid-rich microdomain (ϕ_{peptoid}) affects the positions of the extrema (arising from the $\sin^2(\pi n \phi_A)$ term), and the overall downward trend in intensity with increasing reflection order n is due to the diffuse interface (described by the $e^{-2\pi n^2 (t/d)^2}$ decay factor).

The X-ray scattering contrast in this system ($\Delta\rho$) is dominated by the electron density difference between polystyrene and polypeptoid ($\Delta\rho_{\text{PS–peptoid}} \approx 75$ e$^-$ nm^{-3} and $\Delta\rho_{\text{PnBA–peptoid}} \approx 69$ e$^-$ nm^{-3}) as opposed to the small electron density difference between polar and nonpolar polypeptoid repeat units ($\Delta\rho_{\text{Nme–Npe}} = 1$ e$^-$ nm^{-3}). This simple two-layer model thus captures the majority of the scattering measured, even with variation expected in the distribution of Nme and Npe polypeptoid units within the domains.

RESULTS AND DISCUSSION

A series of polystyrene-*b*-polypeptoid block copolymers with near-symmetric volume fractions was synthesized to understand the role of monomer sequence in interfacial mixing. The polypeptoid block is monodisperse and synthesized as either a homopolymer of polar repeat units (*N*-(methoxyethyl)glycine, Nme) or a precise, sequence-defined copolymer of polar and nonpolar (*N*-(phenylethyl)glycine, Npe) compatibilizing repeat units (Figure 1). Four different sequences with identical composition are studied, each with nine compatibilizing groups: arranged in a forward taper (PS–Taper), arranged in an inverse taper (PS–Inverse), distributed along the chain length (PS–Distributed), or distributed in blocks of three (PS–Blocky).

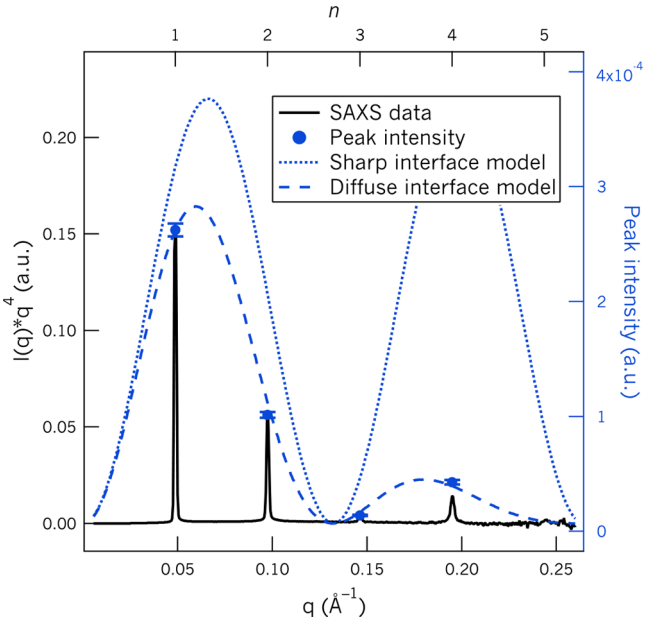

Figure 3. Comparison of sharp interface and diffuse interface models to representative SAXS data (PnBA–Polar). Porod-corrected scattering intensity ($I(q)*q^4$) is plotted versus scattering vector q in black (left, bottom axes). Integrated peak intensities are superimposed as blue markers, along with envelopes representing the fit using the diffuse interface model (dashed blue line) and the sharp interface model with the same volume fraction (dotted blue line) (right, top axes). The diffuse interface is clearly a better model for capturing the measured behavior.

Previous studies of these materials showed sequence-dependent domain spacings and order–disorder transition temperatures, likely influenced by nonideal chain conformations driven by the localization of compatibilizing groups at the polystyrene–polypeptoid interface.[43] This work aims to quantify the mixing of components at that interface via X-ray scattering analysis and simulations with self-consistent field theory.

All samples formed well-ordered, isotropically oriented lamellae (Figure 4) with periods of approximately 10 nm. Interfacial thicknesses (t) were robustly calculated by fitting a diffuse interface model to scattering peak intensities (Table 2).

Effect of Sequence on Interfacial Thickness. With the highest segregation strength[43] the noncompatibilized PS–Polar block copolymer is found to have the smallest interfacial width at 2.51 ± 0.03 nm (Figure 5). When compatibilizing groups are added, the interfacial thickness increases for the tapered sequences but remains narrow for the distributed sequences, despite 25% of the polypeptoid units being replaced with phenyl side chains that promote mixing.

While the SCFT simulations show that the interphase region is 50% polystyrene and 50% polypeptoid for all materials, the proportion of Nme and Npe groups comprising the interfacial polypeptoid depends on the monomer sequence, leading to different amounts of mixing with polystyrene and thus different interfacial thickness. Tracking the locations of polar Nme

https://dx.doi.org/10.1021/acs.macromol.9b02426
Macromolecules 2020, 53, 3262–3272

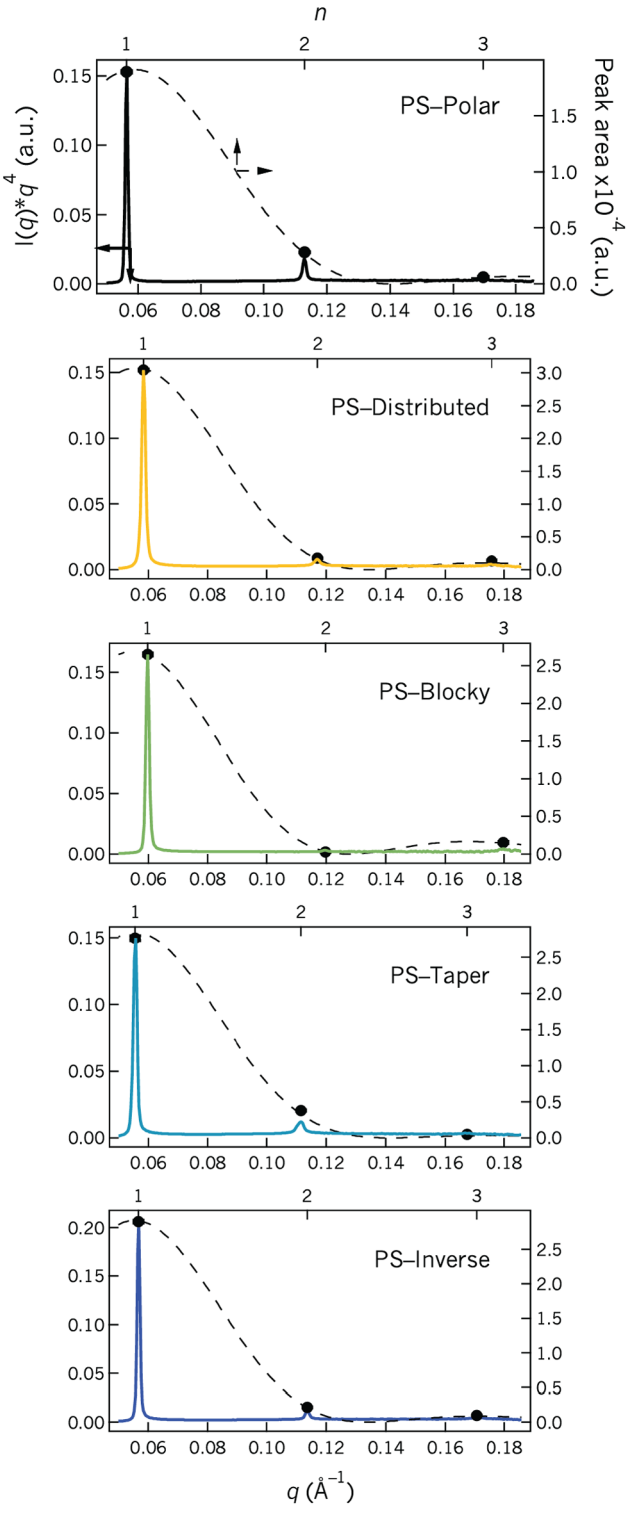

Figure 4. Porod-corrected small-angle X-ray scattering ($I(q)*q^4$) of PS−polypeptoid diblock copolymers (left, bottom axes). Peak areas (markers) fit with a diffuse interface model (dashed lines) are overlaid (right, top axes). Errors in the peak area are smaller than the markers. All diblock copolymers studied form well-ordered lamellae with $2q^*$ and $3q^*$ higher order reflections.

polypeptoid units and nonpolar, compatibilizing Npe units with simulations sheds light on this sequence-dependent mixing at the interface (Figure 6a). For all composition calculations based on SCFT simulations, the interfacial region is defined with eq 5.

The tapered sequences have the highest nonpolar Npe content at the interface, with the interphase of PS−Inverse being composed of 26% Npe units and that of PS−Taper with the highest fraction of Npe units at 29%. (Putting this comparison in terms of individual compatibilizing Npe units in the interphase region: PS−Taper has an extra Npe unit removed from the polypeptoid-rich domain relative to other sequences (Figure 6b).) Correspondingly, the forward-tapered material (PS−Taper) has the largest interfacial thickness (2.97 ± 0.06 nm) followed by the inverse-tapered material (PS−Inverse, 2.78 ± 0.03 nm). This contrasts with prior work on tapered block copolymer systems, where the inverse taper has a larger interfacial thickness than the forward taper.[26] We suspect the difference in interfacial thickness arises from the PS−polypeptoid system having precise monomer sequences with no compositional dispersity and/or a three-component design of PS, Nme, and styrene-like Npe.

In contrast to the tapered sequences, the distributed sequences (PS−Distributed and PS−Blocky) have an interfacial Npe content identical to that of the whole-chain Npe content (25%), i.e., there is no enrichment of Npe units at the interfaces of these materials. While we understand from previous studies that folded chain conformations allow compatibilizing Npe units to migrate toward the interface, the compatibilizing groups are covalently tethered to neighboring polar groups in these distributed sequences, which must accompany them to the interfacial region. This covalent restriction causes the interphase polypeptoid composition of the distributed sequences to reflect the overall composition of 1:3 (i.e., 9:27 Npe:Nme units), as it is not possible to increase local Npe content without also increasing the local Nme content in these sequences. With more polar Nme groups forced to be at the interface there is stronger local repulsion between polypeptoid and polystyrene, causing the narrow interfacial widths of PS−Distributed (2.65 ± 0.06 nm) and PS−Blocky (2.49 ± 0.06 nm). The slightly narrower interface of PS−Blocky versus PS−Distributed likely stems from the larger uninterrupted segments of pure polar repeat units and matches that of the noncompatibilized PS−Polar material. This result suggests the interesting potential for blocky-distributed sequence design to improve processability while maintaining high-fidelity sharp interfaces: PS−Blocky matches the narrow interfacial width of the noncompatibilized material but has an order−disorder temperature that is 62 °C lower. The distribution of the nonpolar polypeptoid groups throughout the polar matrix narrows the interfacial width but promotes mixing in the domains and likely encourages disordering upon heating.

In addition to the quantitative comparisons made with SCFT, a simple scaling argument captures the general trends described above (historically introduced in ref 47). The interface region must be comprised of loops of the two dissimilar polymers in roughly equal amounts, and in a symmetric system there is only one characteristic loop length g. The amount of segmental mixing is determined by the balance of the thermal energy k_BT encouraging mixing and the chemical incompatibility resisting mixing. At equilibrium, the balance of this segmental interaction energy with thermal energy defines a polypeptoid loop (i.e., an interfacial "blob") of g segments that is expected to penetrate the polystyrene domain (and vice versa)

https://dx.doi.org/10.1021/acs.macromol.9b02426
Macromolecules 2020, 53, 3262−3272

Table 2. Self-Assembly Parameters for PS−Polypeptoid Diblock Copolymers[a]

sample	d (nm) (±0.03 nm)	$\phi_{peptoid,calcd}$	$\phi_{peptoid,SAXS}$ (±0.003)	t (nm)	a (nm^2)	$\chi_{eff,t}$ at 150 °C	T_{ODT} (±1 °C)[b]
PS−Polar	11.14	0.40	0.40	2.51 ± 0.03	2.51	0.080	205 °C
PS−Distributed	10.76	0.43	0.43	2.65 ± 0.06	2.76	0.071	143 °C
PS−Blocky	10.51	0.43	0.47	2.49 ± 0.06	3.00	0.081	143 °C
PS−Taper	11.30	0.43	0.39	2.97 ± 0.06	2.45	0.057	151 °C
PS−Inverse	11.06	0.43	0.42	2.78 ± 0.03	2.63	0.068	153 °C

[a]Domain spacing is calculated as $d = 2\pi/q^*$. Volume fraction of the polypeptoid domain ($\phi_{peptoid,SAXS}$) and interfacial thickness (t) are taken from SAXS fits to the diffuse interface model. Interfacial area is calculated as $a = 2v_{chain}/d$. Effective interaction parameter $\chi_{eff,t}$ is approximated using the relationship $t \approx \chi^{-1/2}$. [b]Order−disorder transition temperatures (T_{ODTs}) are reproduced from ref 43 with permission.

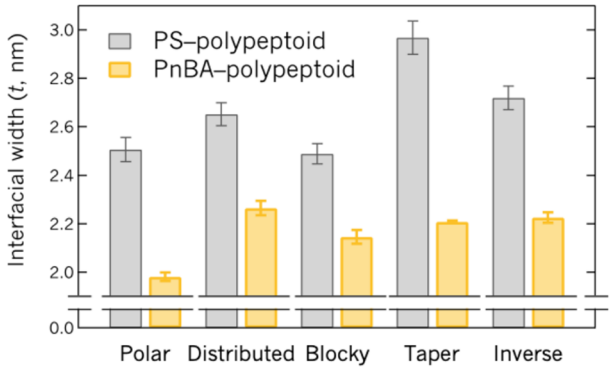

Figure 5. Interfacial widths of lamellar PS−polypeptoid and PnBA−polypeptoid diblock copolymers, calculated from fits of the diffuse interface model (eq 4) to SAXS peak intensities.

$$k_B T \sum_{i=1}^{g} \chi_{PS-peptoid,i} = k_B T \tag{6}$$

where i indexes polypeptoid monomers starting adjacent to the block junction, which are either polar Nme or compatibilizing Npe units, thus defining a sequence-dependent number of segments in the interface, g, and simplifies to

$$\sum_{i=1}^{g} \chi_{PS-peptoid,i} = 1 \tag{7}$$

Assuming the loop of g monomers takes a random walk, the loop radius and thus the interfacial thickness should scale as $t \simeq bg^{1/2}$ with segment length b. Using the same parameters as in the SCFT simulations ($\chi_{PS-Nme}N = 20$ with $N = 86$) and using $\chi_{PS-Npe} = 0.8\chi_{PS-Nme}$ measured previously, we can determine $g^{1/2}$ for each diblock copolymer and calculate a scaling estimate for the interfacial thickness. We find that this scaling approach captures the general trends seen with interfacial thickness measured using SAXS: the polypeptoid loop is calculated to be smallest for PS−Polar and PS−Blocky ($g = 4.3$), which also have the smallest measured interfacial thickness, and largest for PS−Taper ($g = 5.1$), which has the largest interfacial thickness. However, this scaling estimate does not capture all of the behavior measured in this system (the interfacial widths of PS−Distributed and PS−Inverse are reversed with respect to those measured with SAXS). The assumptions of a random walk and equal monomer volume may make this approach less accurate for more subtle differences in sequence. It is known that the portion of the chain near the block junction does not take a true random walk but a stretched one,[64−66] and recent work shows that sequence-defined polymers may deviate from a random walk depending on the sequence of compatibilizing groups.[43] Nonetheless, this simple approach gives an intuitive physical explanation for variation in interfacial thickness with monomer sequence and highlights the importance of the compatibilizing group sequence near the block junction.

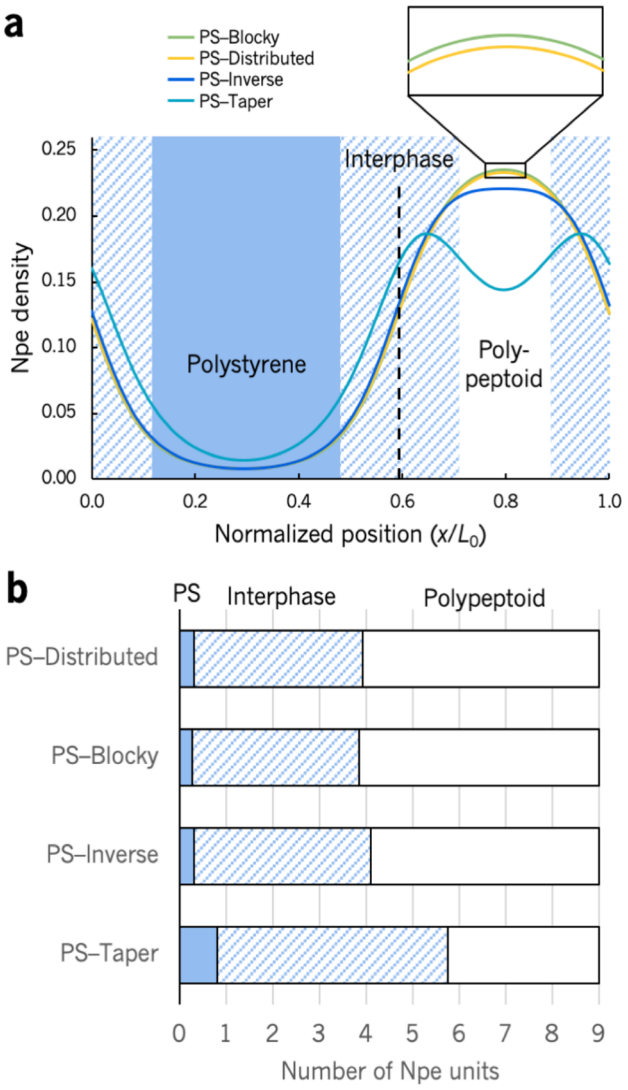

Figure 6. (a) SCFT predictions of the density of Npe compatibilizing units in lamellar domains. (b) Distribution of compatibilizing Npe polypeptoid units in each domain. Tapered sequence PS−Taper has more Npe units in the polystyrene and interfacial regions with fewer Npe units in the polypeptoid domain. Data are shown at $\chi N = 20$.

Sequence Effects on In-Domain Mixing. In addition to interfacial thicknesses, the fits to SAXS data also give the relative sizes of the polystyrene- and polypeptoid-rich domains. Larger polypeptoid-rich domains arise in the distributed

https://dx.doi.org/10.1021/acs.macromol.9b02426
Macromolecules 2020, 53, 3262−3272

sequences, where a higher compatibilizing group content in the center of the domains is found to encourage mixing in of polystyrene, swelling the domain but shrinking the total domain spacing. Overall, the precise placement of compatibilizing groups along the chain is shown to dictate their localization in the self-assembled material at the interface or in the domain centers, where more compatibilizing groups encourage more segmental mixing with polystyrene.

The $\sin^2(n\pi\phi_A)$ term in the lamellar structure factor is very sensitive to volume fraction ϕ_A, so by fitting both interfacial thickness and $\phi_A = \phi_{peptoid,SAXS} < 1/2$, the precise volume fraction of the self-assembled polypeptoid-rich domain can be measured. The volume fractions from SAXS represent the relative sizes of the polypeptoid-rich domain and the PS-rich domain, allowing for mixing and redistribution of components upon self-assembly, not the constant, chain-volume fraction of $\phi_{peptoid} = 0.43$ for the compatibilized series or $\phi_{peptoid} = 0.40$ for PS−Polar.

All polypeptoid-rich domain volume fractions are close to the calculated values (ranging from $\phi_{peptoid,SAXS} = 0.39$ to 0.47 for the compatibilized materials) (Table 2). However, a trend emerges that inversely correlates polypeptoid volume fraction with domain spacing. For example, PS−Taper has the smallest $\phi_{peptoid,SAXS}$ and largest domain spacing, while PS−Blocky has the largest $\phi_{peptoid,SAXS}$ and smallest domain spacing. This inverse relationship is unexpected, as previous work supports the hypothesis that the variation in domain spacing in these materials is a result of sequence-driven collapsed or stretched polypeptoid chain conformations (suggesting that total domain spacing and volume fraction of polypeptoid should trend together).[43] While simulations with SCFT show that chain conformations do indeed vary with sequence, this initial hypothesis does not incorporate mixing of polystyrene into the polypeptoid domain and vice versa. For all samples, SCFT shows that there is no region of the self-assembled lamellae that is "pure" polypeptoid or polystyrene—there is significant mixing even far from the interface. While PS−polypeptoid is a fairly high-χ system ($\chi_{PS-Nme} \approx 0.08$ using reference volume $v_0 = 0.1$ nm^3 with little temperature dependence),[43] the block copolymers studied here are relatively small ($N \approx 100$), so the segregation strength (χN) is much less than 100 and therefore far from the strong segregation limit. With a relatively low χN, we expect a fair amount of mixing between polypeptoid and polystyrene at the interface and for the center of the lamellar microdomains to contain some amount of the other block. In fact, simulations show that at $\chi_{PS-Nme}N = 20$, the domain centers are composed of 5−10% of the opposite block species. Further, this "in-domain" mixing is not equivalent between the two domains: there is more polystyrene in the polypeptoid-rich domain than there is polypeptoid in the polystyrene-rich domain. This is emphasized at lower segregation strengths and is shown at $\chi_{PS-Nme}N = 15$ in Figure 7a. Asymmetric in-domain mixing shifts some volume of polystyrene into the polypeptoid domain, swelling the polypeptoid domain and increasing the measured $\phi_{peptoid,SAXS}$. This phenomenon has been previously observed in a forward-tapered PS−PI copolymer system, where segmental intermixing occurred more extensively in the polystyrene-rich region than the polyisoprene-rich region.[9,10] In this study, PS−Blocky has the most in-domain mixing (asymmetrically favored in the polypeptoid-rich region) and also the largest positive deviation from the calculated polypeptoid volume fraction, suggesting that polystyrene is mixing with the compatibilizing Npe groups distributed throughout the polypeptoid domain and swelling it (Figure 7b and 7c). Of the compatibilized materials, PS−Taper has the least in-domain mixing and the largest negative deviation from the calculated polypeptoid volume fraction, suggesting that polystyrene is avoiding mixing with the more pure (polar) polypeptoid domain and is more strongly localized in the polystyrene domain, which expands the total domain spacing.

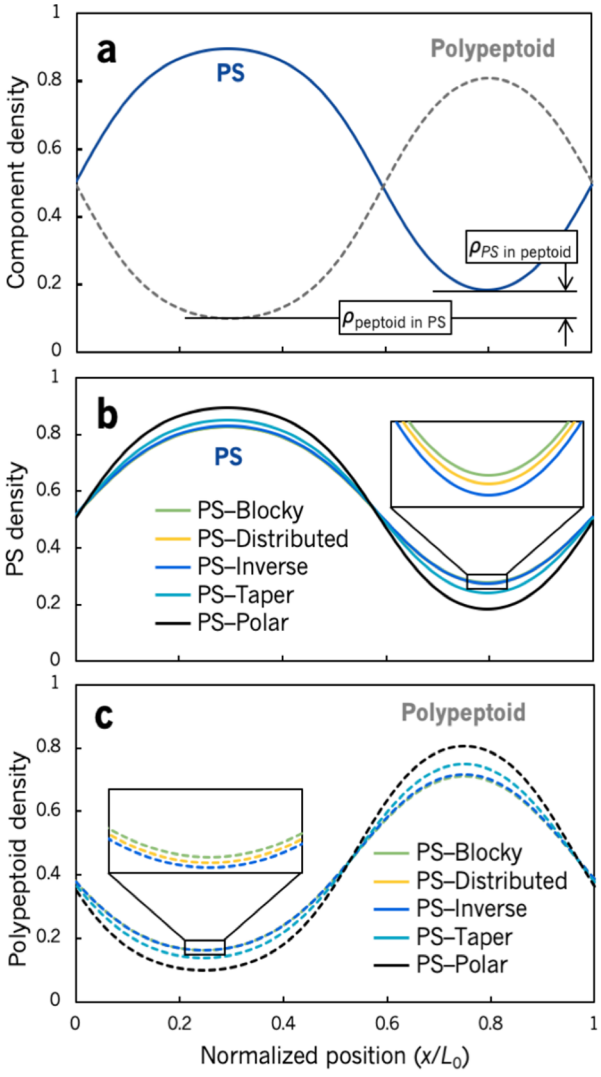

Figure 7. Self-consistent field theory simulations at $\chi_{PS-Nme}N = 15$. (a) Overall composition profiles for polystyrene and polypeptoid (example shown is PS−Polar). There is more intermixing of PS into the polypeptoid domain than polypeptoid into the PS domain. (b) Total polystyrene density and (c) polypeptoid density for different sequences. Insets show expanded views of the minima that are most similar to each other. In-domain mixing decreases from PS−Blocky to PS−Polar in the order of the legend; there is more in-domain mixing for the distributed sequences and less for the tapered sequences, with PS−Polar having the least.

The variation in composition at the interface further suggests variation in an effective interaction parameter calculated at the interfacial region ($\chi_{eff,t}$). Assuming the simplest relationship of $t \sim \chi^{-1/2}$, a sequence-independent scaling factor, and using the previously measured χ_{PS-Nme} as a reference,[43] we can compute the effective interfacial χ of a sequence-defined block copolymer from the ratio of the measured interfacial thicknesses ($\chi_2 \sim \chi_1\left(\frac{t_1}{t_2}\right)^2$) calculated at

https://dx.doi.org/10.1021/acs.macromol.9b02426
Macromolecules 2020, 53, 3262−3272

150 °C and summarized in Table 2. These effective χ parameters are included to illustrate trends in the behavior, rather than present thorough quantitative values. By examining the trend in these $\chi_{eff,t}$, it is apparent that they do not follow the relative order of order−disorder transition temperatures measured previously. For example, PS−Blocky has one of the lowest order−disorder transition temperatures but has a high effective χ parameter matching that of PS−Polar, which has an order−disorder transition temperature ∼60 °C higher. A better predictor for the order−disorder transition temperature in this system is in-domain mixing: where the more blended distributed sequences have lower order−disorder transition temperatures and the more demixed tapered sequences have higher disordering temperatures. Estimating χ solely from interfacial width inherently relies on the local composition at the interface, while here simulation shows that the composition at the interface varies with sequence (Figure 6). Thus, we find for these sequence-defined materials that not only is interfacial mixing important for thermodynamic properties but also the in-domain mixing emphasized above is important too.

In summary, variation in monomer sequence affects both interfacial mixing, leading to differences in interfacial width, and in-domain mixing, leading to differences in domain volume fractions. Simulations with SCFT reveal that the primary sequence determines the distribution of compatibilizing groups throughout the self-assembled domains, which modulates mixing at the interface and results in asymmetric distributions of materials in the domain centers (Figure 8). Tapered

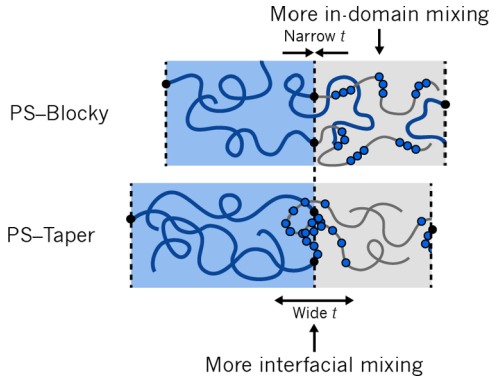

Figure 8. Monomer sequence determines the degree of interfacial and in-domain mixing, leading to variation in interfacial thickness and volume fraction.

sequences, especially the forward-tapered PS−Taper, have enriched compatibilizing group content at the interface, leading to more mixing and broader interfacial widths but suppressed in-domain mixing of polystyrene due to the higher local content of polar polypeptoid units, shrinking the polypeptoid-rich domain volume fraction. Distributed sequences, especially the blocky-distributed PS−Blocky, have fewer compatibilizing groups at the interface, leading to narrowed interfacial widths, but promote in-domain mixing of polystyrene into the polypeptoid-rich domain, expanding the polypeptoid-rich volume fraction. The combination of interfacial and in-domain mixing determines the final self-assembled structure, but it is found that in-domain mixing likely dominates the thermal stability.

Comparison to a Higher χ System. To study the effects of interaction parameter χ on the interfacial width, an analogous series was synthesized with poly(*n*-butyl acrylate) (PnBA) conjugated to the same five polypeptoid blocks shown in Figure 1 (molecular characteristics are listed in Table 1, and SAXS data is shown in Figure SI-4). The nonpolar Npe polypeptoid repeat unit is expected to also compatibilize the polar polypeptoid to the relatively nonpolar PnBA. Application of the random phase approximation to PnBA−Polar and PS−Polar indicates that the PnBA series has a slightly higher χ than the PS series (Figures 9 and SI-5).

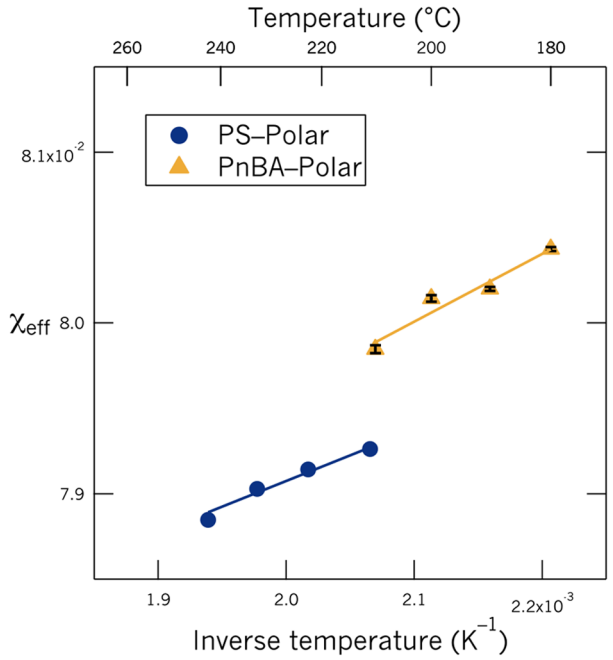

Figure 9. Effective interaction parameters (χ_{eff}s) for PS−Polar and PnBA−Polar diblock copolymers, as measured through application of the random phase approximation to disordered scattering curves.

The PnBA−polypeptoid interfacial thicknesses are ∼0.5 nm (∼15−20%) smaller than the PS−polypeptoid analogues (Figure 5 and Table 3) in all cases except PnBA−Taper, which has measurable excess polypeptoid and therefore a narrowed interfacial width (see Figures SI-1 and SI-2). Overall, the same trends with sequence are seen in this higher χ series but with smaller absolute differences between sequences due to the smaller interfacial widths.

While the measured difference in χ is small, the large differences in interfacial width suggest difference in χ should be larger. Following the simplest relationship of $t \sim \chi^{-1/2}$, the effective χ determined by the interfacial widths of the PnBA series should be ∼1.1 times that of the PS series, while the χs measured via RPA reflect a ratio of just ∼1.01. This discrepancy may point to a chemistry-dependent prefactor.

This comparison shows that sequence design has a greater potential for tuning the interfacial width in lower χ systems, while the higher χ systems approach the same narrow interfacial width regardless of sequence.

CONCLUSIONS

This work demonstrates that monomer sequence significantly impacts the thermodynamics of mixing at both the interfaces and the centers of self-assembled block copolymer nanodomains, quantified with structure factor analysis of small-angle X-ray scattering and simulations with self-consistent field

https://dx.doi.org/10.1021/acs.macromol.9b02426
Macromolecules 2020, 53, 3262−3272

Table 3. Self-Assembly Parameters for PnBA−Polypeptoid Diblock Copolymers[a]

sample	d (nm) (±0.03 nm)	$\phi_{peptoid,calcd}$ (±0.003)	$\phi_{peptoid,SAXS}$	t (nm)
PnBA−Polar	12.89	0.40	0.37	1.98 ± 0.02
PnBA−Distributed	11.98	0.42	0.40	2.26 ± 0.03
PnBA−Blocky	12.03	0.42	0.40	2.15 ± 0.03
PnBA−Taper	12.15	0.42	(0.37)	(2.21 ± 0.01)
PnBA−Inverse	12.07	0.42	0.40	2.22 ± 0.02

[a]Values in parentheses are depressed by excess polypeptoid.

theory. At the interface, tapered sequences are enriched in compatibilizing groups, enhancing interfacial mixing and broadening the interfacial width, while the domain centers are more pure and have suppressed mixing. Distributed sequences have sharp interfaces due to the necessity of neighboring polar groups accompanying compatibilizing groups to the interface, but the forced mixing of polar and nonpolar peptoid units in the polypeptoid-rich domain promotes polystyrene mixing into the domain center and swells the domain. The combination of these effects—interfacial mixing and in-domain mixing—demonstrates the rich behavior of sequence-defined polymers and the ability to tune morphological properties with monomer sequence alone.

■ ASSOCIATED CONTENT

Supporting Information

The Supporting Information is available free of charge at https://pubs.acs.org/doi/10.1021/acs.macromol.9b02426.

GPC and MALDI data for poly(*n*-butyl acrylate)−polypeptoid and polystyrene−polypeptoid diblock copolymers and constituent blocks, and SAXS data for poly(*n*-butyl acrylate)−polypeptoid diblock copolymers (PDF)

■ AUTHOR INFORMATION

Corresponding Author

Rachel A. Segalman − *Materials Department and Department of Chemical Engineering, University of California, Santa Barbara, California 93106, United States;* orcid.org/0000-0002-4292-5103; Email: segalman@ucsb.edu

Authors

Anastasia L. Patterson − *Materials Department, University of California, Santa Barbara, California 93106, United States;* orcid.org/0000-0003-3875-1195

Beihang Yu − *Department of Chemical Engineering, University of California, Santa Barbara, California 93106, United States;* orcid.org/0000-0001-5060-0766

Scott P. O. Danielsen − *Department of Chemical Engineering, University of California, Santa Barbara, California 93106, United States;* orcid.org/0000-0003-3432-5578

Emily C. Davidson − *Department of Chemical Engineering, University of California, Santa Barbara, California 93106, United States*

Glenn H. Fredrickson − *Materials Department, Department of Chemical Engineering, and Materials Research Laboratory, University of California, Santa Barbara, California 93106, United States;* orcid.org/0000-0002-6716-9017

Complete contact information is available at: https://pubs.acs.org/10.1021/acs.macromol.9b02426

Author Contributions

The manuscript was written through contributions of all authors. All authors have given approval to the final version of the manuscript.

Notes

The authors declare no competing financial interest.

■ ACKNOWLEDGMENTS

The authors gratefully acknowledge funding from the National Science Foundation (NSF) Division of Materials Research program (DMR-1608297) for all experimental work and the NSF Condensed Matter and Materials Theory Program (DMR-1822215) for self-consistent field theory simulations. A.L.P. gratefully acknowledges the NSF for a graduate research fellowship. We gratefully thank Rachel Behrens for assistance with polypeptoid characterization and block copolymer purification and acknowledge use of the MRL Shared Experimental Facilities, supported by the MRSEC Program of the NSF, a member of the NSF-funded Materials Research Facilities Network (DMR-1720256). SCFT simulations utilized resources of the Center for Scientific Computing (DMR-1720256) and NSF (CNS-1725797). X-ray scattering was performed at the National Synchrotron Light Source II, a U.S. Department of Energy Office of Science User Facility (DE-SC0012704; beamline 11-BM), and the Advanced Light Source, a DOE Office of Science User Facility (DE-AC02-05CH11231; beamline 7.3.3). The authors thank Bryan Beckingham (University of Auburn) for helpful discussions regarding extracting interfacial widths from X-ray scattering, Nicole Schauser and Seamus Jones for supplemental X-ray scattering, and Ron Zuckermann (Molecular Foundry, Lawrence Berkeley National Lab) for helpful discussions regarding polypeptoid synthesis.

■ REFERENCES

(1) Eagan, J. M.; Xu, J.; Di Girolamo, R.; Thurber, C. M.; Macosko, C. W.; LaPointe, A. M.; Bates, F. S.; Coates, G. W. Combining polyethylene and polypropylene: Enhanced performance with PE/iPP multiblock polymers. *Science* **2017**, *355* (6327), 814−816.

(2) Xu, J.; Eagan, J. M.; Kim, S. S.; Pan, S.; Lee, B.; Klimovica, K.; Jin, K. L.; Lin, T. W.; Howard, M. J.; Ellison, C. J.; LaPointe, A. M.; Coates, G. W.; Bates, F. S. Compatibilization of Isotactic Polypropylene (iPP) and High-Density Polyethylene (HDPE) with iPP-PE Multiblock Copolymers. *Macromolecules* **2018**, *51* (21), 8585−8596.

(3) Macosko, C. W.; Guegan, P.; Khandpur, A. K.; Nakayama, A.; Marechal, P.; Inoue, T. Compatibilizers for melt blending: Premade block copolymers. *Macromolecules* **1996**, *29* (17), 5590−5598.

(4) Eastwood, E. A.; Dadmun, M. D. Multiblock copolymers in the compatibilization of polystyrene and poly(methyl methacrylate) blends: Role of polymer architecture. *Macromolecules* **2002**, *35* (13), 5069−5077.

(5) Creton, C.; Kramer, E. J.; Hui, C. Y.; Brown, H. R. Failure Mechanisms of Polymer Interfaces Reinforced with Block Copolymers. *Macromolecules* **1992**, *25* (12), 3075−3088.
(6) Dai, K. H.; Kramer, E. J. Molecular-Weight Dependence of Diblock Copolymer Segregation at a Polymer-Polymer Interface. *J. Polym. Sci., Part B: Polym. Phys.* **1994**, *32* (11), 1943−1950.
(7) Schmolka, I. R. Review of Block Polymer Surfactants. *J. Am. Oil Chem. Soc.* **1977**, *54* (3), 110−116.
(8) Shen, M.; Kaelble, D. H. On Viscoelastic Behavior of a Styrene-Butadiene-Styrene (S-B-S) Block Copolymer. *J. Polym. Sci., Part B: Polym. Lett.* **1970**, *8* (3), 149−153.
(9) Hashimoto, T.; Tsukahara, Y.; Tachi, K.; Kawai, H. Structure and Properties of Tapered Block Polymers.4. Domain-Boundary Mixing and Mixing-In-Domain Effects on Microdomain Morphology and Linear Dynamic Mechanical Response. *Macromolecules* **1983**, *16* (4), 648−657.
(10) Hashimoto, T.; Tsukahara, Y.; Kawai, H. Structure And Properties Of Tapered Block Polymers Of Styrene And Isoprene.2. Dynamic Mechanical Responses And Their Structural Interpretations. *Polym. J.* **1983**, *15* (10), 699−711.
(11) Ruiz, R.; Wan, L.; Lopez, R.; Albrecht, T. R. Line Roughness in Lamellae-Forming Block Copolymer Films. *Macromolecules* **2017**, *50* (3), 1037−1046.
(12) Sunday, D. F.; Maher, M. J.; Hannon, A. F.; Liman, C. D.; Tein, S.; Blachut, G.; Asano, Y.; Ellison, C. J.; Willson, C. G.; Kline, R. J. Characterizing the Interface Scaling of High chi Block Copolymers near the Order-Disorder Transition. *Macromolecules* **2018**, *51* (1), 173−180.
(13) Lee, K. S.; Lee, J.; Kwak, J.; Moon, H. C.; Kim, J. K. Reduction of Line Edge Roughness of Polystyrene-block-Poly(methyl methacrylate) Copolymer Nanopatterns By Introducing Hydrogen Bonding at the Junction Point of Two Block Chains. *ACS Appl. Mater. Interfaces* **2017**, *9* (37), 31245−31251.
(14) Kennemur, J. G.; Yao, L.; Bates, F. S.; Hillmyer, M. A. Sub-5 nm Domains in Ordered Poly(cyclohexylethylene)-block-poly(methyl methacrylate) Block Polymers for Lithography. *Macromolecules* **2014**, *47* (4), 1411−1418.
(15) Azuma, K.; Sun, J.; Choo, Y.; Rokhlenko, Y.; Dwyer, J. H.; Schweitzer, B.; Hayakawa, T.; Osuji, C. O.; Gopalan, P. Self-Assembly of an Ultrahigh-chi Block Copolymer with Versatile Etch Selectivity. *Macromolecules* **2018**, *51* (16), 6460−6467.
(16) Sinturel, C.; Bates, F. S.; Hillmyer, M. A. High chi-Low N Block Polymers: How Far Can We Go? *ACS Macro Lett.* **2015**, *4* (9), 1044−1050.
(17) Luo, Y. D.; Montarnal, D.; Treat, N. J.; Hustad, P. D.; Christianson, M. D.; Kramer, E. J.; Fredrickson, G. H.; Hawker, C. J. Enhanced Block Copolymer Phase Separation Using Click Chemistry and Ionic Junctions. *ACS Macro Lett.* **2015**, *4* (12), 1332−1336.
(18) Tirumala, V. R.; Daga, V.; Bosse, A. W.; Romang, A.; Ilavsky, J.; Lin, E. K.; Watkins, J. J. Well-Ordered Polymer Melts with 5 nm Lamellar Domains from Blends of a Disordered Block Copolymer and a Selectively Associating Homopolymer of Low or High Molar Mass. *Macromolecules* **2008**, *41* (21), 7978−7985.
(19) Luo, Y. D.; Kim, B.; Montarnal, D.; Mester, Z.; Pester, C. W.; McGrath, A. J.; Hill, G.; Kramer, E. J.; Fredrickson, G. H.; Hawker, C. J. Improved Self-Assembly of Poly(dimethylsiloxane-b-ethylene oxide) Using a Hydrogen-Bonding Additive. *J. Polym. Sci., Part A: Polym. Chem.* **2016**, *54* (14), 2200−2208.
(20) Teran, A. A.; Balsara, N. P. Thermodynamics of Block Copolymers with and without Salt. *J. Phys. Chem. B* **2014**, *118* (1), 4−17.
(21) Loo, W. S.; Sethi, G. K.; Teran, A. A.; Galluzzo, M. D.; Maslyn, J. A.; Oh, H. J.; Mongcopa, K. I.; Balsara, N. P. Composition Dependence of the Flory-Huggins Interaction Parameters of Block Copolymer Electrolytes and the Isotaksis Point. *Macromolecules* **2019**, *52* (15), 5590−5601.
(22) Perry, S. L.; Sing, C. E. 100th Anniversary of Macromolecular Science Viewpoint: Opportunities in the Physics of Sequence-Defined Polymers. *ACS Macro Lett.* **2020**, *9* (2), 216−225.
(23) Singh, N.; Tureau, M. S.; Epps, T. H., III Manipulating ordering transitions in interfacially modified block copolymers. *Soft Matter* **2009**, *5* (23), 4757−4762.
(24) Roy, R.; Park, J. K.; Young, W. S.; Mastroianni, S. E.; Tureau, M. S.; Epps, T. H., III Double-Gyroid Network Morphology in Tapered Diblock Copolymers. *Macromolecules* **2011**, *44* (10), 3910−3915.
(25) Mastroianni, S. E.; Epps, T. H., III Interfacial Manipulations: Controlling Nanoscale Assembly in Bulk, Thin Film, and Solution Block Copolymer Systems. *Langmuir* **2013**, *29* (12), 3864−3878.
(26) Luo, M.; Brown, J. R.; Remy, R. A.; Scott, D. M.; Mackay, M. E.; Hall, L. M.; Epps, T. H. Determination of Interfacial Mixing in Tapered Block Polymer Thin Films: Experimental and Theoretical Investigations. *Macromolecules* **2016**, *49* (14), 5213−5222.
(27) Kim, J.; Gray, M. K.; Zhou, H. Y.; Nguyen, S. T.; Torkelson, J. M. Polymer blend compatibilization by gradient copolymer addition during melt processing: Stabilization of dispersed phase to static coarsening. *Macromolecules* **2005**, *38* (4), 1037−1040.
(28) Kim, J.; Mok, M. M.; Sandoval, R. W.; Woo, D. J.; Torkelson, J. M. Uniquely broad glass transition temperatures of gradient copolymers relative to random and block copolymers containing repulsive comonomers. *Macromolecules* **2006**, *39* (18), 6152−6160.
(29) Wong, C. L. H.; Kim, J.; Torkelson, J. M. Breadth of glass transition temperature in styrene/acrylic acid block, random, and gradient copolymers: Unusual sequence distribution effects. *J. Polym. Sci., Part B: Polym. Phys.* **2007**, *45* (20), 2842−2849.
(30) Mok, M. M.; Pujari, S.; Burghardt, W. R.; Dettmer, C. M.; Nguyen, S. T.; Ellison, C. J.; Torkelson, J. M. Microphase separation and shear alignment of gradient copolymers: Melt rheology and small-angle X-ray scattering analysis. *Macromolecules* **2008**, *41* (15), 5818−5829.
(31) Seo, Y.; Brown, J. R.; Hall, L. M. Effect of Tapering on Morphology and Interfacial Behavior of Diblock Copolymers from Molecular Dynamics Simulations. *Macromolecules* **2015**, *48* (14), 4974−4982.
(32) Brown, J. R.; Seo, Y. M.; Sides, S. W.; Hall, L. M. Unique Phase Behavior of Inverse Tapered Block Copolymers: Self Consistent Field Theory and Molecular Dynamics Simulations. *Macromolecules* **2017**, *50* (14), 5619−5626.
(33) Ganesan, V.; Kumar, N. A.; Pryamitsyn, V. Blockiness and Sequence Polydispersity Effects on the Phase Behavior and Interfacial Properties of Gradient Copolymers. *Macromolecules* **2012**, *45* (15), 6281−6297.
(34) Rosales, A. M.; Murnen, H. K.; Zuckermann, R. N.; Segalman, R. A. Control of Crystallization and Melting Behavior in Sequence Specific Polypeptoids. *Macromolecules* **2010**, *43* (13), 5627−5636.
(35) Rosales, A. M.; McCulloch, B. L.; Zuckermann, R. N.; Segalman, R. A. Tunable Phase Behavior of Polystyrene-Polypeptoid Block Copolymers. *Macromolecules* **2012**, *45* (15), 6027−6035.
(36) Rosales, A. M.; Segalman, R. A.; Zuckermann, R. N. Polypeptoids: a model system to study the effect of monomer sequence on polymer properties and self-assembly. *Soft Matter* **2013**, *9* (35), 8400−8414.
(37) Davidson, E. C.; Rosales, A. M.; Patterson, A. L.; Russ, B.; Yu, B. H.; Zuckermann, R. N.; Segalman, R. A. Impact of Helical Chain Shape in Sequence-Defined Polymers on Polypeptoid Block Copolymer Self-Assembly. *Macromolecules* **2018**, *51* (5), 2089−2098.
(38) van Zoelen, W.; Zuckermann, R. N.; Segalman, R. A. Tunable Surface Properties from Sequence-Specific Polypeptoid-Polystyrene Block Copolymer Thin Films. *Macromolecules* **2012**, *45* (17), 7072−7082.
(39) Sun, J.; Stone, G. M.; Balsara, N. P.; Zuckermann, R. N. Structure-Conductivity Relationship for Peptoid-Based PEO-Mimetic Polymer Electrolytes. *Macromolecules* **2012**, *45* (12), 5151−5156.
(40) Sun, J.; Teran, A. A.; Liao, X. X.; Balsara, N. P.; Zuckermann, R. N. Nanoscale Phase Separation in Sequence-Defined Peptoid Diblock Copolymers. *J. Am. Chem. Soc.* **2013**, *135* (38), 14119−14124.
(41) Sun, J.; Teran, A. A.; Liao, X. X.; Balsara, N. P.; Zuckermann, R. N. Crystallization in Sequence-Defined Peptoid Diblock Copolymers

https://dx.doi.org/10.1021/acs.macromol.9b02426
Macromolecules 2020, 53, 3262−3272

Induced by Microphase Separation. *J. Am. Chem. Soc.* **2014**, *136* (5), 2070−2077.
(42) Sun, J.; Liao, X. X.; Minor, A. M.; Balsara, N. P.; Zuckermann, R. N. Morphology-Conductivity Relationship in Crystalline and Amorphous Sequence-Defined Peptoid Block Copolymer Electrolytes. *J. Am. Chem. Soc.* **2014**, *136* (42), 14990−14997.
(43) Patterson, A. L.; Danielsen, S. P. O.; Yu, B.; Davidson, E. C.; Fredrickson, G. H.; Segalman, R. A. Sequence Effects on Block Copolymer Self-Assembly through Tuning Chain Conformation and Segregation Strength Utilizing Sequence-Defined Polypeptoids. *Macromolecules* **2019**, *52* (3), 1277−1286.
(44) Semenov, A. N. Theory of Block-Copolymer Interfaces in the Strong Segregation Limit. *Macromolecules* **1993**, *26* (24), 6617−6621.
(45) Shull, K. R. Mean-Field Theory of Block Copolymers: Bulk Melts, Surfaces, and Thin Films. *Macromolecules* **1992**, *25* (8), 2122−2133.
(46) Ohta, T.; Kawasaki, K. Equilibrium Morphology of Block Copolymer Melts. *Macromolecules* **1986**, *19* (10), 2621−2632.
(47) Helfand, E.; Tagami, Y. Theory of Interface between Immiscible Polymers. *J. Chem. Phys.* **1972**, *57* (4), 1812.
(48) Burns, A. B.; Christie, D.; Mulhearn, W. D.; Register, R. A. Estimating the segregation strength of microphase-separated diblock copolymers from the interfacial width. *J. Polym. Sci., Part B: Polym. Phys.* **2019**, *57* (14), 932−940.
(49) Gruendling, T.; Junkers, T.; Guilhaus, M.; Barner-Kowollik, C. Mark-Houwink Parameters for the Universal Calibration of Acrylate, Methacrylate and Vinyl Acetate Polymers Determined by Online Size-Exclusion Chromatography-Mass Spectrometry. *Macromol. Chem. Phys.* **2010**, *211* (5), 520−528.
(50) Zuckermann, R. N.; Kerr, J. M.; Kent, S. B. H.; Moos, W. H. Efficient Method for the Preparation of Peptoids [Oligo(N-substituted glycines)] by Submonomer Solid-Phase Synthesis. *J. Am. Chem. Soc.* **1992**, *114* (26), 10646−10647.
(51) Ilavsky, J. Nika: software for two-dimensional data reduction. *J. Appl. Crystallogr.* **2012**, *45*, 324−328.
(52) Fredrickson, G. H. *The Equilibrium Theory of Inhomogeneous Polymers*; Oxford Science Publications: Oxford, UK, 2006.
(53) Barrat, J. L.; Fredrickson, G. H.; Sides, S. W. Introducing variable cell shape methods in field theory simulations of polymers. *J. Phys. Chem. B* **2005**, *109* (14), 6694−6700.
(54) Rasmussen, K. O.; Kalosakas, G. Improved numerical algorithm for exploring block copolymer mesophases. *J. Polym. Sci., Part B: Polym. Phys.* **2002**, *40* (16), 1777−1783.
(55) Tzeremes, G.; Rasmussen, K. O.; Lookman, T.; Saxena, A. Efficient computation of the structural phase behavior of block copolymers. *Phys. Rev. E: Stat. Phys., Plasmas, Fluids, Relat. Interdiscip. Top.* **2002**, *65* (4), 041806−1−5.
(56) Ceniceros, H. D.; Fredrickson, G. H. Numerical solution of polymer self-consistent field theory. *Multiscale Model. Simul.* **2004**, *2* (3), 452−474.
(57) Roe, R.-J. *Methods of X-Ray and Neutron Scattering in Polymer Science*; Oxford University Press: New York, 2000.
(58) Beckingham, B. S.; Register, R. A. Architecture-Induced Microphase Separation in Nonfrustrated A-B-C Triblock Copolymers. *Macromolecules* **2013**, *46* (9), 3486−3496.
(59) Ruland, W. Small-Angle Scattering of 2-Phase Systems - Determination and Significance of Systematic Deviations from Porods Law. *J. Appl. Crystallogr.* **1971**, *4* (Feb1), 70−73.
(60) Hashimoto, T.; Shibayama, M.; Kawai, H. Domain-Boundary Structure of Styrene-Isoprene Block Co-Polymer Films Cast from Solution.4. Molecular-Weight Dependence of Lamellar Microdomains. *Macromolecules* **1980**, *13* (5), 1237−1247.
(61) Shibayama, M.; Hashimoto, T. Small-Angle X-Ray-Scattering Analyses of Lamellar Microdomains Based on a Model of One-Dimensional Paracrystal with Uniaxial Orientation. *Macromolecules* **1986**, *19* (3), 740−749.
(62) Cser, F. About the Lorentz correction used in interpretation of small-angle X-ray scattering data of semicrystalline polymers. *J. Appl. Polym. Sci.* **2001**, *80* (3), 358−366.
(63) Ruland, W. Integral Width of Convolution of a Gaussian and a Cauchy Distribution. *Acta Crystallogr.* **1965**, *18*, 581.
(64) Matsushita, Y.; Mori, K.; Saguchi, R.; Noda, I.; Nagasawa, M.; Chang, T.; Glinka, C. J.; Han, C. C. Chain Conformations and Locations of Parts of a Block Polymer in a Lamellar Structure. *Macromolecules* **1990**, *23* (20), 4387−4391.
(65) Kim, S. H.; Jo, W. H. A Monte Carlo simulation of polymer polymer interface in the presence of block copolymer. I. Effects of the chain length of block copolymer and interaction energy. *J. Chem. Phys.* **1999**, *110* (24), 12193−12201.
(66) Hasegawa, H.; Tanaka, H.; Hashimoto, T.; Han, C. C. Sans and Saxs Studies on Molecular-Conformation of a Block Polymer in Microdomain Space.2. Contrast Matching Technique. *Macromolecules* **1987**, *20* (9), 2120−2127.

https://dx.doi.org/10.1021/acs.macromol.9b02426
Macromolecules 2020, 53, 3262−3272